Terr. Atmos. Ocean. Sci., Vol. 32, No. 6, Part I, 989-999, December 2021 doi: 10.3319/TAO.2021.11.08.02

Intensive GNSS radio occultation observations by FORMOSAT-7/COSMIC-2 in the dawn, noon, dusk, and midnight ionosphere

Po-Han Lee[1], Jann-Yenq Liu[1, 2, 3, *], Chi-Yen Lin[1, 2], and Fu-Yuan Chang[2]

[1] *Department of Space Science and Engineering, National Central University, Taoyuan City, Taiwan*
[2] *Center for Astronautical Physics and Engineering, National Central University, Taoyuan City, Taiwan*
[3] *Center for Space and Remote Sensing Research, National Central University, Taoyuan City, Taiwan*

Article history:
Received 31 May 2021
Revised 11 October 2021
Accepted 8 November 2021

Keywords:
FORMOSAT-7/COSMIC-2, Intensive observation, GNSS, Radio occultation, NmF2, hmF2

Citation:
Lee, P.-H., J.-Y. Liu, C.-Y. Lin, and F.-Y. Chang, 2021: Intensive GNSS radio occultation observations by FORMOSAT-7/COSMIC-2 in the dawn, noon, dusk, and midnight ionosphere. Terr. Atmos. Ocean. Sci., 32, 989-999, doi: 10.3319/TAO.2021.11.08.02

ABSTRACT

Intensive GNSS radio occultation (RO) observations by side-by-side 6 satellites of FORMOSAT-7/COSMIC-2 (F7/C2) are used to study the high temporal and fine spatial resolution of the three-dimensional structures and dynamics of the electron density in the equatorial and low-latitude ionosphere. Five events are selected to study signatures at dawn, noon, dusk, and midnight sectors using the measurements taken during a one-month period. We also construct a reference of diurnal variations of the F2-peak height (hmF2) and electron density (NmF2) with 47642 profiles within ±7.5° magnetic latitude in June to August during 2006 - 2010 observed by FORMOSAT-3/COSMIC (F3/C). Good agreements between F7/C2 and F3/C show that the intensive GNSS RO observation can be used to promptly examine the sunrise effect, quasi-equilibrium distribution, pre-reversal enhancement, and midnight magnetosphere-ionosphere coupling at the dawn, noon, dusk, and midnight period, respectively.

1. INTRODUCTION

The FORMOSAT-7/COSMIC-2 (F7/C2) satellites were launched by SpaceX Falcon Heavy rocket on 25 June 2019, at Kennedy Space Center, Florida, USA (https://www.nspo.narl.org.tw/inprogress.php?c=20022301&ln=en). All six satellites of the F7/C2 constellation were first parked at a 720-km circular orbit during a 1-month period of 25 June to 24 July 2019. These satellites were gradually transferred to their mission orbits at 550 km altitude with an inclination angle of 24 degrees and an orbital period of about 97 minutes from 24 July 2019 to 31 January 2021. F7/C2 is equipped with a GNSS receiver, which can receive GPS signals from the United States and GLONASS signals from Russia. By measuring radio occultation (RO) signals, atmospheric temperature and humidity, as well as ionospheric total electron content (TEC) can be derived. The Abel inversion (Hajj and Romans 1998) has been employed to invert and the electron density (Ne) profiles from the RO TEC profiles. These TEC and Ne profiles allow us to have a better understanding of three-dimensional (3D) structures and dynamics of ionospheric plasma (Lin et al. 2007; Liu et al. 2010; Lee et al. 2011; Chang et al. 2015, 2020). During this intensive observation period, simultaneous GNSS RO profiles sounded by 5 - 6 next adjacent F7/C2 satellites provide a once-in-a-lifetime opportunity to study fine structures of 3D Ne in the low-latitude ionosphere with high temporal resolution. The temporal and spatial sounding ranges around the F2 peak of the F7/C2 satellites are about 5 - 7 minutes and 40 - 190 km. In total, 173 events have been observed during the period (Fig. 1). Here, we report fine 3D Ne structures and dynamics at dawn, noon, dusk, and midnight by means of the F7/C2 incursive observations.

2. OBSERVATION AND RESULT

There are 173 intensive observation events occurring

* *Corresponding author*
E-mail: tigerjyliu@gmail.com

in the 1-month intense observation period of 25 June to 24 July 2019 (F10.7: 68 - 70 sfu, solar flux unit, a convenient measure of spectral flux density often used in solar radio observations) (Fig. 1). We select five events at four-time sectors at dawn, noon, dusk, and midnight to study the response of Ne to sunrise, quasi-equilibrium distribution, pre-reversal enhancement (PRE), and plasma transportations/irregularity (Ratcliffe 1972; Farley et al. 1986; Davies 1990; Kelley 2009), respectively. For each time sector, one event is selected, except that two selected events are employed to examine Ne changes in the early and late phases of PRE. Table 1 lists the location, local time (LT), and day of the five events. To compare the five events with previous long-term observations, we construct a reference of diurnal variations of the F2-peak height (hmF2) and electron density (NmF2) with 47642 profiles, within ±7.5° magnetic latitude, in the months period of June to August during the low solar activity years from April 2006 to December 2010 (F10.7: 65 - 103 sfu) observed by FORMOSAT 3/COSMIC (F3/C) (Fig. 2).

For studying the sunrise effect, we examine TEC and Ne profiles sounded by the six F7/C2 satellites of #5, #6, #2, #4, #1, and #3 at 1.7°N, -108.8°E (6.7°N geomagnetic) at 0608 LT (8 minutes prior to the local sunrise at 0616 LT on the ground) on 21 July 2019 (Figs. 3a and b). These sequential profiles reveal that the TEC- and F2-peak appear at about 200 and 220 km, respectively. The six satellites descending southward observe 3D Ne structures (Fig. 3c). Figures 3d and e depict that NmF2 increases from 1.02×10^5 to 1.33×10^5 # cm^{-3}, while hmF2 descends from 226.9 to 221.8 km within a horizontal range of 40.9 km during a 455-second sounding duration. Figure 3d illustrates that the NmF2 of F7/C2 increases smoothly (black dashed curve), which is similar to that of F3/C (grey dashed curve), and comparing to a smoothly descending of the F3/C hmF2 (grey solid curve), the hmF2 of F7/C2 yields a descending trend with small structures (black solid curve). Assuming the ionosphere to be horizontally stratified, we can compute the time rate of electron density changes ($\partial Ne/\partial t$) at a certain altitude during the sounding period (Appendix A). Figure 3f shows that Ne prominently increases between 200 - 300 km altitude, especially around the F2-peak height, but slightly increases above 400 km altitude. The percentage of the change to its ambient electron density is a small value, which varies from 0.007 to 0.06%.

To assess the midday effect, we study TEC and Ne profiles sounded by F7/C2 satellite #5, #2, #4, #1, and #3 at 25.2°N, 7.2°E (14.42°N geomagnetic) during the post noon period at 1239 LT (39 minutes after the local noon of 1200 LT on the ground) on 21 July 2019 (Figs. 4a and b). These sequential profiles reveal that the TEC- and F2-peak appear at about 240 and 280 km, respectively. The F7/C2 satellites ascending northward observe 3D Ne structures (Fig. 4c). Figures 4d and e depict that NmF2 increases from 2.84×10^5 to 2.93×10^5 # cm^{-3} and hmF2 fluctuates over a small altitude range between 273.5 and 276.5 km within a horizontal distance of 210 km during the 479-second event period. Figure 4d illustrates that variations in NmF2 and hmF2 of F7/C2 and F3/C are small, which meet the quasi-equilibrium distribution of the ionosphere. Similar to Fig. 3d, small perturbations appear in the F7/C2 hmF2. Figure 4f displays that the time rate of changes of Ne is about small values of 0 - 20 # cm^{-3} s^{-1} at 250 - 300 km altitude and becomes -20 # cm^{-3} s^{-1} below 200 km altitude. F7/C2 satellite #5, #2, #4, #1, and #3 observe that below 200 km altitude, the TEC increase correspondingly; however, the Ne oppositely decrease. Therefore, the time variation of electron density is negative below ~250 km, which could be due to the retrieval error of the Abel inversion. Nevertheless, the percentage of the change to its ambient electron density is a small value of about 0, which confirms the whole ionosphere is right under the quasi-equilibrium distribution.

To study the PRE signatures, events before and after the local sunset are selected. During the early PRE phase, Fig. 5 displays the TEC and Ne profiles observed at -0.8°N, -95.2°E (7.6°N geomagnetic) around the pre-sunset period at 1752 LT (50 minutes prior to the local sunset on the ground at 1842 LT) on 20 July 2019. The sequential profiles sounded by F7/C2 satellites #5, #6, #4, #1, and #3 reveal that the TEC- and F2-peak appear at about 280 and 300 km, respectively (Figs. 5a and b). The 5 F7/C2 satellites ascending northward sound 3D Ne structures (Fig. 5c). Figures 5d and e depict that NmF2 decreases from 5.34×10^5 to 4.2×10^5 # cm^{-3} while hmF2 ascends from 289.3 to 303.1 km within a horizontal distance of 193.6 km during a 428-second duration. It is interesting to find that NmF2 and hmF2 of F3/C are almost constant values, which might result from a large amount of data that have been taken the average. By contrast, the intensive observation of F7/C2 observes the ionospheric variations within a very short duration and distance. Figure 5f shows that Ne rapidly decreases between 200 - 350 km altitude, especially below the F2-peak height, and however no obvious Ne temporal changes can be found above 400 km altitude. The percentages of the change to the ambient electron density are small negative values, varying from -0.11 to -0.002%.

For the later PRE phase, Fig. 6 illustrates the TEC and Ne profiles observed at 7.4°N, -31.3°E (2.6°N geomagnetic) during the post-sunset period at 1954 LT (87 minutes after the local sunset on the ground at 1827 LT) on 18 July 2019. The sequential profiles sounded by F7/C2 satellite #6, #2, #4, #1, and #3 reveal that the TEC- and F2-peak appear at about 250 and 280 km, respectively (Figs. 6a and b). The 5 F7/C2 satellites ascending southward sound 3D Ne structures (Fig. 6c). Figures 6d and e depict that NmF2 decreases from 1.96×10^5 to 1.86×10^5 # cm^{-3}, while hmF2 descends from 260.9 to 249.1 km within the horizontal distance of 142.5 km during a 312-second duration. NmF2 of F3/C and

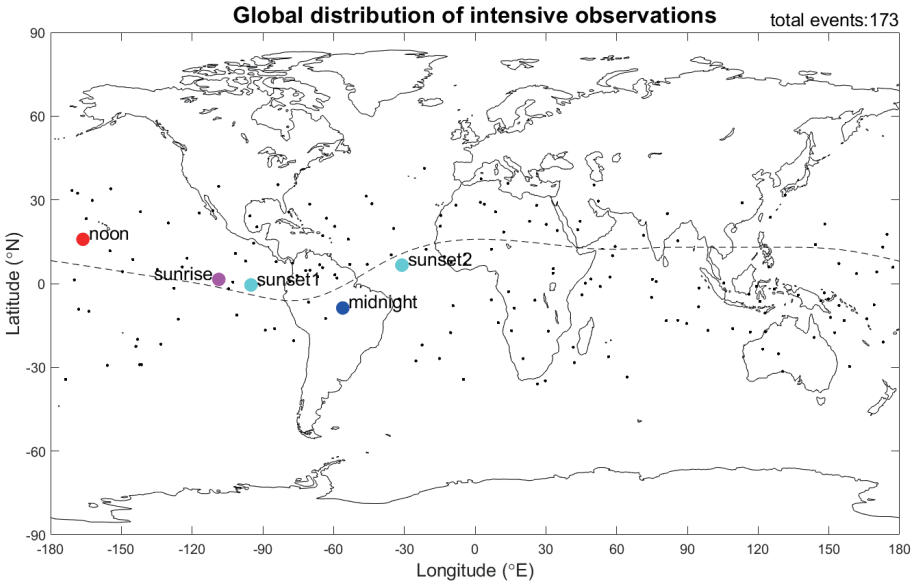

Fig. 1. Locations of the intensive observations probe by F7/C2.

Table 1. Information of Five Selected Events.

Event	Local time	Locations (°N, °E)	Magnetic (°N)	Date
Sunrise	0608	(1.7, -108.8)	6.7	21 July 2019
Noon	1239	(25.2, 7.2)	14.2	21 July 2019
Sunset1	1752	(-0.8, -95.2)	7.6	20 July 2019
Sunset2	1954	(7.4, -31.3)	2.6	18 July 2019
Midnight	2323	(-8.9, -56.3)	-0.5	19 July 2019

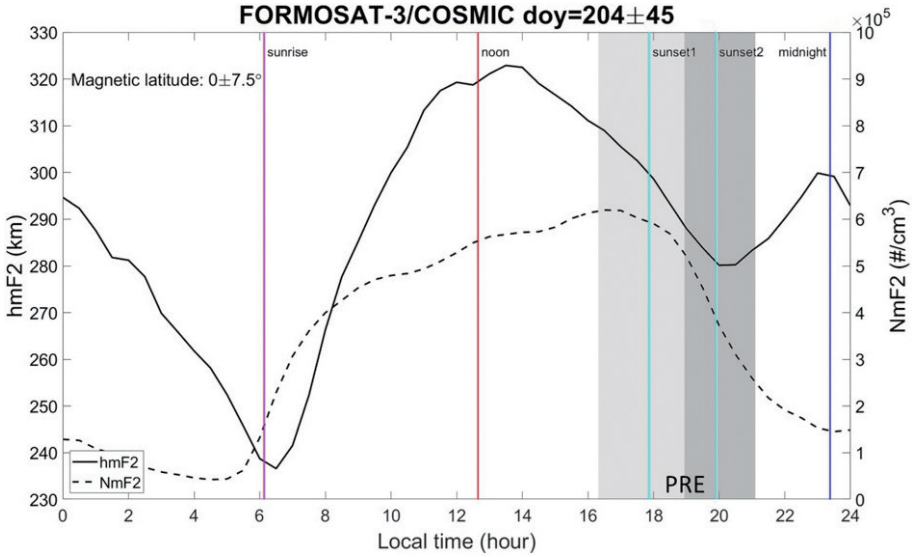

Fig. 2. The diurnal variation of hmF2 (solid curve) and NmF2 (dashed curve) observed by F3/C at magnetic latitude between -7.5 to 7.5 during April 2006 to December 2010. Duration of the early and late phase of the pre-reversal enhancement are marked with light and dark gray rectangular, respectively. The NmF2 and hmF2 values are the medians of all longitude sector of the globe.

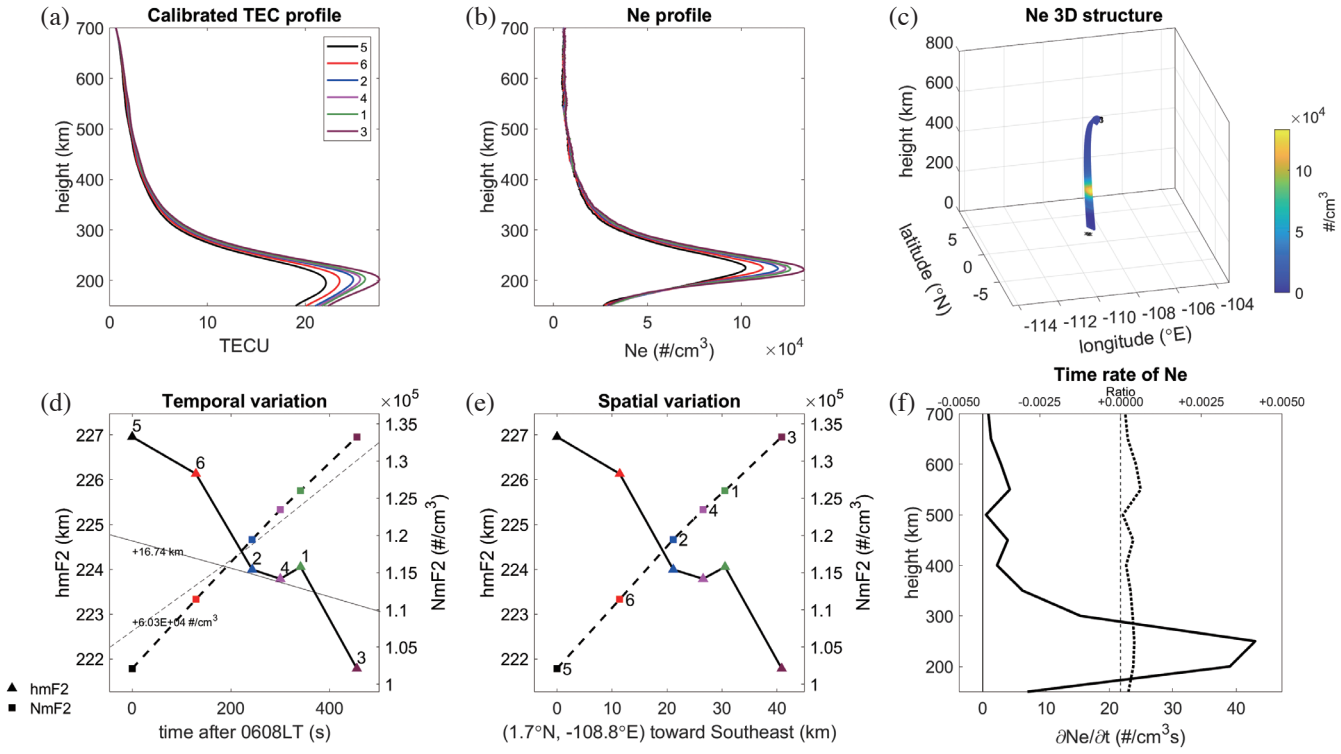

Fig. 3. F7/C2 ionospheric GNSS RO observations at 1.7°N, -108.8°E (6.7°N geomagnetic) during sunrise period of 0608 LT on 21 July 2019. Sunrise time: 0618 LT (a) Calibrated TEC profiles. (b) Electron density profiles. (c) 3D electron density. (d) The temporal variation of hmF2 (triangle) and NmF2 (square) from 0608 LT toward sunrise. The solid and dashed curves stand for the corresponding hmF2 and NmF2 derived from F3/C observations, respectively. Note that NmF2 and hmF2 of F3/C have been offset to compare with those of F7/C2. (e) The spatial variation of hmF2 and NmF2 from (1.7°N, -108.8°E) southeast toward the sunrise line. (f) The time rate of electron density changes and the percentage of the change to its ambient electron density from 200 to 700 km. Vertical solid and dashed lines stand for $\partial Ne/\partial t$ and the ratio being zero. The colors and numbers denote the number of the F7/C2 satellites.

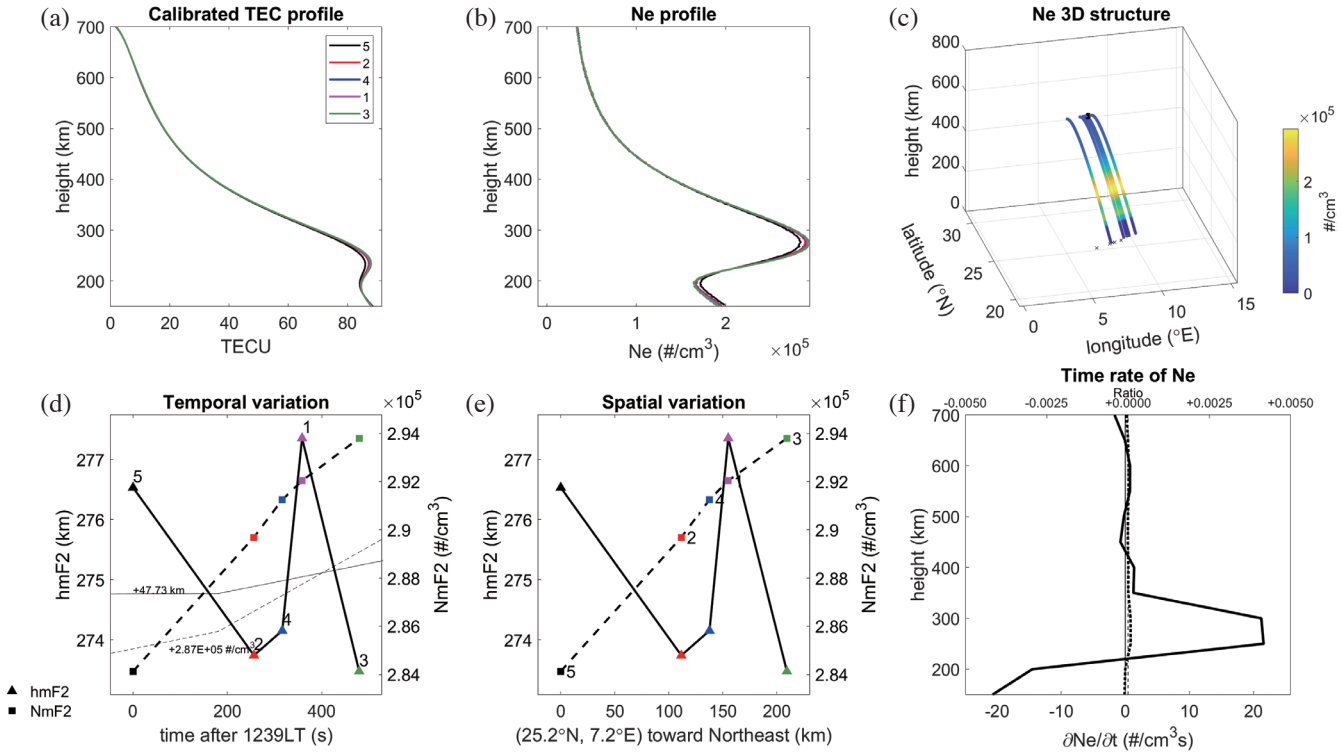

Fig. 4. Same as Fig. 3 but for the F7/C2 GNSS RO intensive observations at 25.2°N, 7.2°E at noon of 1239 LT on 21 July 2019.

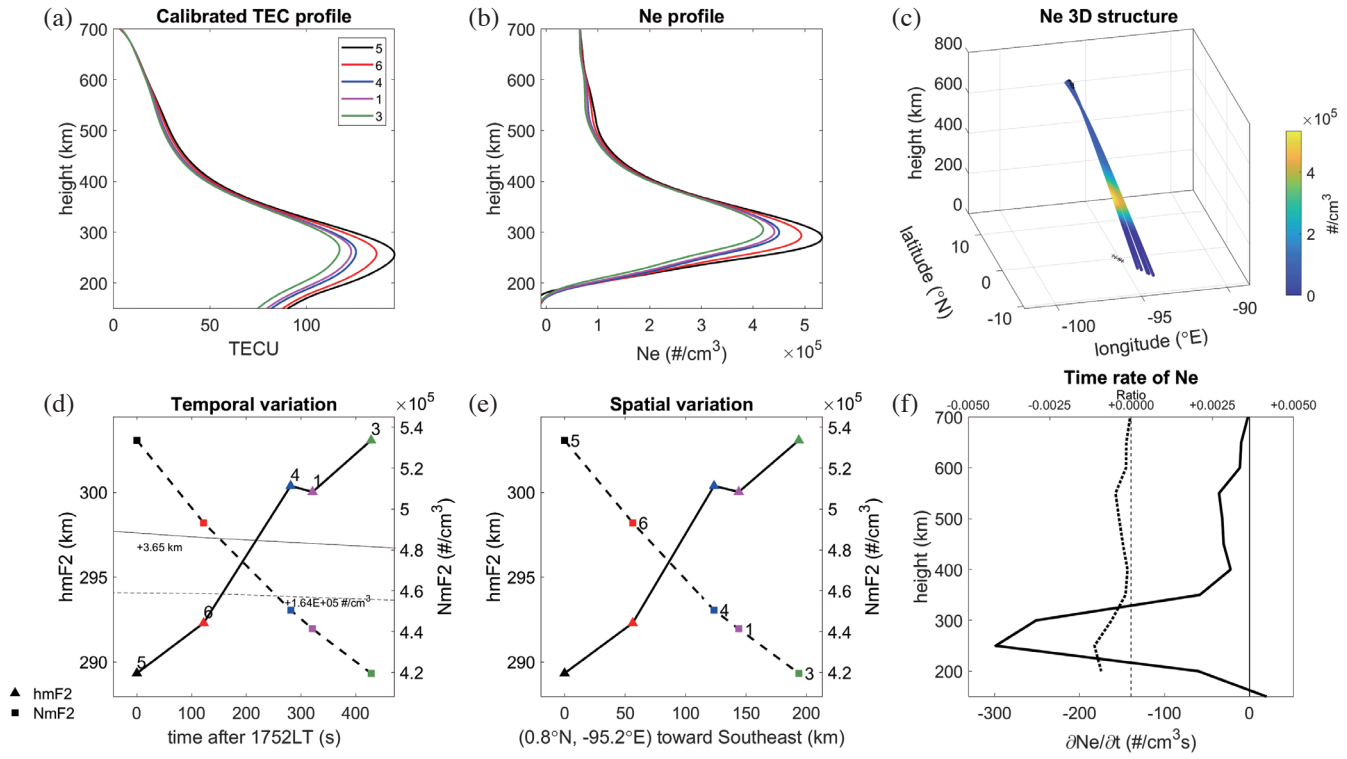

Fig. 5. Same as Fig. 3 but for the F7/C2 GNSS RO intensive observations at 0.8°N, -95.2°E during sunset period of 1752 LT on 20 July 2019. Sunset time: 1842 LT. (f) Owing to the retrieval error of the Abel inversion, Ne is negative and $\partial Ne/\partial t$ is not plotted below 200 km altitude.

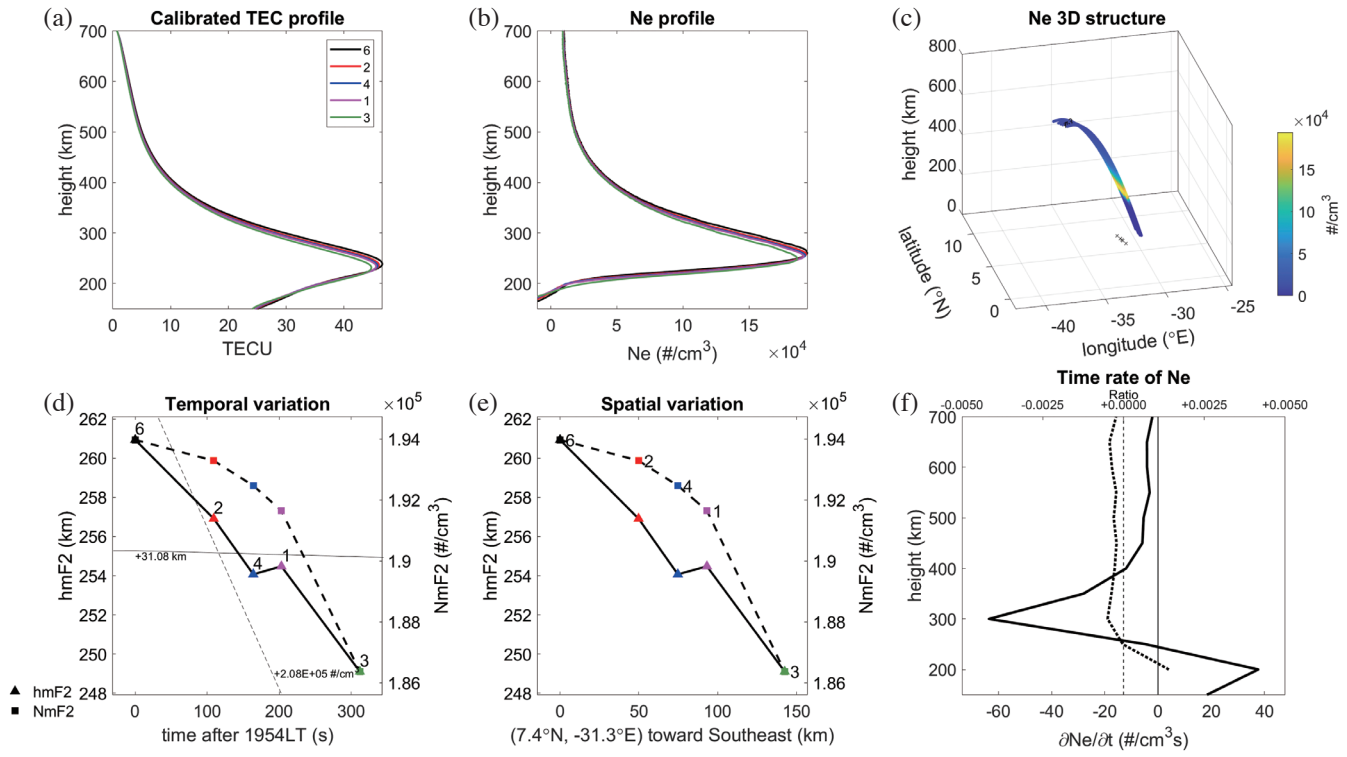

Fig. 6. Same as Fig. 3 but for the F7/C2 GNSS RO intensive observations at 7.4°N, -31.3°E during sunset period of 1954 LT on 18 July 2019. Sunset time: 1827 LT. (f) Owing to the retrieval error of the Abel inversion, Ne is negative and $\partial Ne/\partial t$ is not plotted below 200 km altitude.

F7/C2 yield nearly identical tendencies while hmF2 of F3/C is almost constant values and that of F7/C2 monotonically decreases. Figure 6f shows that Ne rapidly decreases between 250 - 375 km altitude. The time rate of Ne changes is slightly larger than zero above 400 km altitude. The percentages of the change to the ambient electron density are small negative values of -0.05 to -0.002%, except below 250 km altitude.

For the midnight ionosphere, the TEC and Ne profiles are observed at -8.9°N, -56.3°E (7.6°N geomagnetic) during pre-midnight period at 2323 LT (37 minutes prior to the local midnight on the ground at 0000 LT) on 19 July 2019. The sequential profiles sounded by F7/C2 satellite #5, #6, #2, #4, and #3 reveal that the TEC- and F2-peak appear at about 270 and 290 km, respectively (Figs. 7a and b). Figure 7b shows significant density fluctuations compared with the density observations at different periods. These density fluctuations may be related to the nighttime ionospheric irregularities (e.g., equatorial plasma bubble) since the increase of ionospheric layer height during midnight could increase the growth rate of the bubble (Nishioka et al. 2012). Equatorial plasma bubbles usually can cause significant electron density fluctuations; small electron density fluctuations could be due to the decrease of background electron density during midnight (Fig. 7c). Figures 7d and e depict that NmF2 decreases from 4.73×10^4 to 4.27×10^4 # cm^{-3}, while hmF2 ascends from 280.9 to 294.1 km within a horizontal distance of 60.6 km during a 403-second duration. NmF2 of F3/C and F7/C2 yield nearly identical tendencies while hmF2 of F3/C is almost constant values and that of F7/C2 monotonically increases. In general, NmF2 of F3/C and F7/C2 have similar temporal tendencies; however, possibly due to taking the median over the six years period of 2006 - 2010, hmF2 of F3/C yields nearly constant values. By contrast, the F7/C2 intensive observations observe hmF2 changes within a very short duration. Figure 7f shows that the time rate of Ne changes is mostly negative. The percentages of the change to the ambient electron density are mainly negative values of -0.27 to -0.008 %, except around 350 km altitude. The percentages being large negative values around 200 km altitude might result from the loss processes in the lower part ionosphere, while the percentage being positive might be due to the downward diffusion from the topside ionosphere around the midnight period.

3. DISCUSSION AND CONCLUSION

The ionosphere is formed in the Earth's upper atmosphere by incident solar radiation interacting with, and removing electrons, from different gases. The time rate of electron density changes $\frac{\partial Ne}{\partial t}$ is a function of the production rate (Q), the loss rate (L), and the transport $\nabla \cdot (N_e \vec{V})$, which can be expressed as (Ratcliffe 1972; Davies 1990),

$$\frac{\partial Ne}{\partial t} = Q - L - \nabla \cdot (Ne\vec{V}) \quad (1)$$

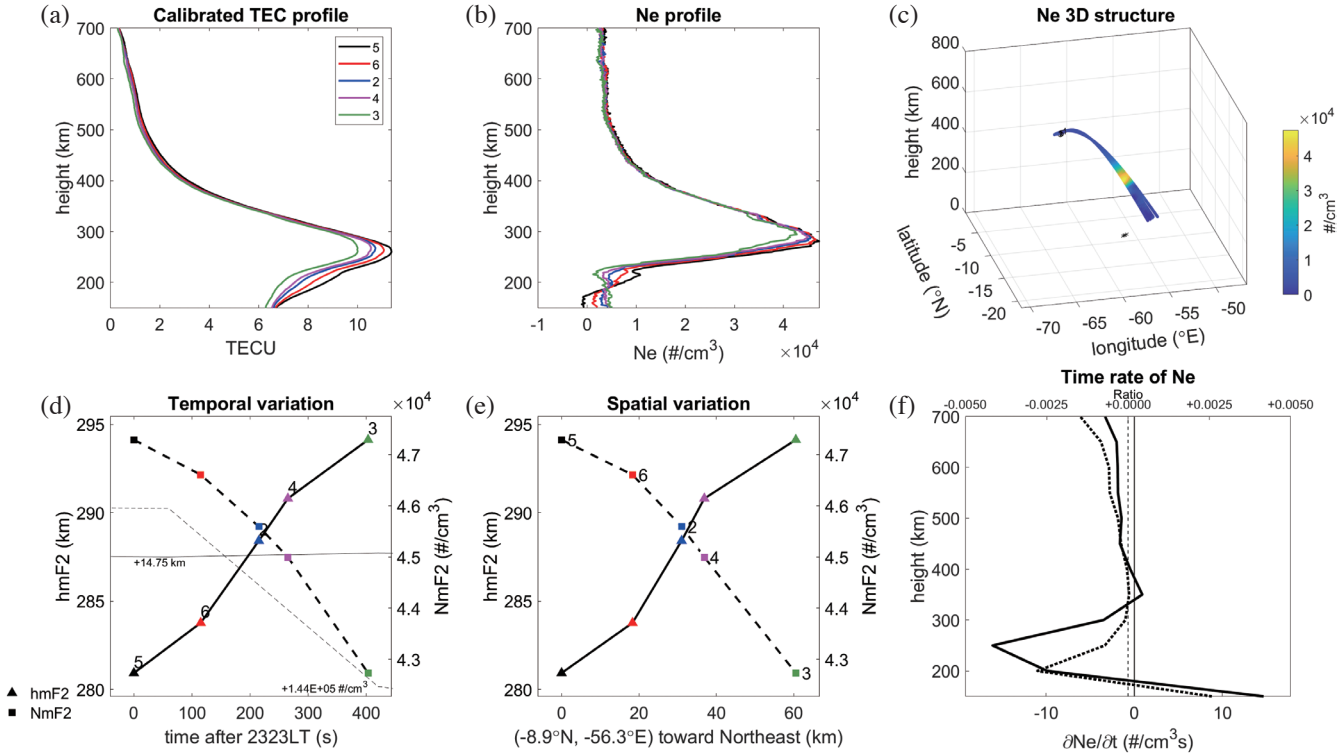

Fig. 7. Same as Fig. 3 but for the F7/C2 GNSS RO intensive observations at -8.9°N, -56.3°E at midnight of 2323 LT on 19 July 2019.

where Q and L are the photochemical processes mainly due to solar ionizations and ion-electron recombination, respectively. Therefore, the events at dawn, noon, dusk, and midnight are used to examine the response of the ionosphere to rapid increase of solar radiation, quasi-equilibrium distribution, rapid decrease of solar radiation together with PRE, and downward diffusions from the magnetosphere, respectively.

Well agreements between F7/C2 and F3/C observations show that due to rapid solar radiation increases NmF2 monotonically increase but hmF2 descends right before the local sunrise (Figs. 2 and 3d). Again, owing to the rapid increase in solar radiations, the time rate of electron density changes in the whole ionosphere are all positive (Fig. 3f), which indicates that Ne of the whole ionosphere increases. Based on the Chapman distribution (Chapman 1931), the height and the magnitude of the Q maximum are functions of the solar zenith angle. The larger zenith angle results in the higher altitude and the lower rate of the Q maximum. Around the midday, where the zenith angle is small, the height of the Q maximum generally is around 120 km altitude, and therefore it requires strong upward diffusions to transport the electron to a higher altitude, such as the F-region about 300 km altitude (Ratcliffe 1972; Davies 1990). The event is observed 10 minutes before the local sunrise on the ground, where the zenith angle is greater than 90°. Although it is before sunrise, the topside ionosphere might have already experienced solar radiations (Rishbeth and Setty 1961; Prabhakaran Nayar et al. 2009). Because solar radiations shine the ionosphere from the top to down, even without any strong upward diffusions, the electron density increases in the whole ionosphere, especially around 200 - 300 km altitude (Fig. 3f).

During the day, as the sun rises and sets, the rate of production by the solar radiation at any level increases to a maximum and then decreases: at some stage the resulting electron density also reaches a maximum, so that $\frac{\partial Ne}{\partial t} = 0$, which is termed the quasi-equilibrium distribution. Thus, an event around noon provides a good chance to study the quasi-equilibrium distribution, such as Fig. 4. F7/C2 and F3/C observations show that NmF2s yield the constant value and hmF2s are at the same altitude (Figs. 2, 4d, and e). The time rate of Ne changes, $\frac{\partial Ne}{\partial t}$, in Fig. 4f is about zero and yields the smallest value below 350 km among Figs. 3f - 6f. Moreover, the percentages of the change to the ambient electron density are about zero in Fig. 4f, which confirms that the whole ionosphere is under the quasi-equilibrium distribution during the midday.

Owing to the eastward and westward electric fields increasing right before and after about the sunset, vertical plasma velocities at the early and late phase of PRE are upward and downward, respectively (Farley et al. 1986). These result in that the ionosphere ascends and the electron density in the lower ionosphere decreases during the PRE early phase, and the ionosphere descends during the PRE late phase. Figures 5d and e show that F7/C2 hmF2 drastically ascends and F7/C2 NmF2 significantly decreases in the PRE early phase, which are much more intense than those of F3/C. Figure 5f shows that the time rate of electron density changes at all the altitudes are in negative, which indicates the electron density decreases in the whole ionosphere during the PRE early phase. For the PRE late phase, owing to the downward plasma flows, hmF2 quickly descends and NmF2 rapidly decreases (Figs. 6d and e). Since there are no solar radiations and the loss process becomes essential after the sunset, the electron density continuously decreases in all altitudes, except that below 250 km altitude, where receive the downward plasma diffusion. Again, tendencies of NmF2 and hmF2 of F7/C2 and F3/C are similar, except the F3/C being less intense.

Since no solar radiations, the loss process in the low ionosphere and downward plasma flows from the magnetosphere become dominant during midnight. F3/C observations depict that in general, hmF2 can shortly vary from ascending to descending, while NmF2 decreases prior to midnight (Fig. 2). Figures 7d and e show that for the F7/C2 intensive midnight observation, NmF2 decreases and hmF2 ascends. Figure 7f reveals that due to the loss process, the electron density of the ionosphere generally decreases slightly.

Based on a large amount of data of 47642 profiles within ±7.5° magnetic latitude observed in the long-term period of June-August during 2006 - 2010 (1000 days) observed by F3/C, the diurnal variation in the median value of hmF2 and NmF2 along the magnetic equator can be obtained. Although such a large amount of data has been used, it still has difficulty obtaining the 3D structure of the ionospheric electron density in detail. By contrast, the F7/C2 intensive observation allows us to examine 3D electron density structure and dynamics with very high time and fine spatial resolution during a very short time interval (i.e., event duration) of about 300 - 500 sec. Tendencies and variations of hmF2 and NmF2 of F7/C2 in the five events generally agree well with those of the F3/C reference, but the former is much more intense than the latter. This is because the former ones are obtained by a signal event of the intensive observation, while the latter ones are the medians calculated from the large amount of data. In conclusion, based on the results of the F7/C2 intensive observation, it is worthy of having a mission with several next adjacent satellites to observe fine plasma structures and dynamics of the ionosphere.

Acknowledgements The authors gratefully acknowledge the NSPO and Taiwan Analysis Center for COSMIC (TACC) for providing FORMOSAT-7/COSMIC-2 and FORMOSAT-3/COSMIC data (https://tacc.cwb.gov.tw/v2/en/index.html). This study is supported by the Taiwan Ministry of Science and Technology (MOST) grant MOST 109-2111-M-008-008. This work was financially supported

partially by the Center for Astronautical Physics and Engineering (CAPE) from the Featured Area Research Center program within the framework of Higher Education Sprout Project by the Ministry of Education (MOE) in Taiwan.

REFERENCES

Chang, F. Y., J. Y. Liu, L. C. Chang, C. H. Lin, and C. H. Chen, 2015: Three-dimensional electron density along the WSA and MSNA latitudes probed by FORMOSAT-3/COSMIC. *Earth Planets Space*, **67**, 156, doi: 10.1186/s40623-015-0326-8. [Link]

Chang, F. Y., J. Y. Liu, T. W. Fang, P. K. Rajesh, and C. H. Lin, 2020: Plasma depletion bays in the equatorial ionosphere observed by FORMOSAT-3/COSMIC during 2007–2014. *J. Geophys. Res.*, **125**, e2019JA027501, doi: 10.1029/2019JA027501. [Link]

Chapman, S., 1931: The absorption and dissociative or ionizing effect of monochromatic radiation in an atmosphere on a rotating earth. *Proc. Phys. Soc. Lond.*, **43**, 26-45, doi: 10.1088/0959-5309/43/1/305. [Link]

Davies, K., 1990: Ionospheric Radio, IEE Electromagnetic Wave Series, Vol. 31, Peter Peregrinus Ltd., London, 600 pp, doi: 10.1049/PBEW031E. [Link]

Farley, D. T., E. Bonelli, B. G. Fejer, and M. F. Larsen, 1986: The prereversal enhancement of the zonal electric field in the equatorial ionosphere. *J. Geophys. Res.*, **91**, 13723-13728, doi: 10.1029/JA091iA12p13723. [Link]

Hajj, G. A. and L. J. Romans, 1998: Ionospheric electron density profiles obtained with the Global Positioning System: Results from the GPS/MET experiment. *Radio Sci.*, **33**, 175-190, doi: 10.1029/97RS03183. [Link]

Kelley, M. C., 2009: The Earth's Ionosphere: Plasma Physics and Electrodynamics, 2nd Edition, Academic Press, Boston, 576 pp.

Lee, I. T., W. Wang, J. Y. Liu, C. Y. Chen, and C. H. Lin, 2011: The ionospheric midlatitude trough observed by FORMOSAT-3/COSMIC during solar minimum. *J. Geophys. Res.*, **116**, A06311, doi: 10.1029/2010JA015544. [Link]

Lin, C. H., C. C. Hsiao, J. Y. Liu, and C. H. Liu, 2007: Longitudinal structure of the equatorial ionosphere: Time evolution of the four-peaked EIA structure. *J. Geophys. Res.*, **112**, A12305, doi: 10.1029/2007JA012455. [Link]

Liu, J. Y., C. Y. Lin, C. H. Lin, H. F. Tsai, S. C. Solomon, Y. Y. Sun, I. T. Lee, W. S. Schreiner, and Y. H. Kuo, 2010: Artificial plasma cave in the low-latitude ionosphere results from the radio occultation inversion of the FORMOSAT-3/COSMIC. *J. Geophys. Res.*, **115**, A07319, doi: 10.1029/2009JA015079. [Link]

Nishioka, M., Y. Otsuka, K. Shiokawa, T. Tsugawa, Effendy, P. Supnithi, T. Nagatsuma, and K. T. Murata, 2012: On post-midnight field-aligned irregularities observed with a 30.8-MHz radar at a low latitude: Comparison with *F*-layer altitude near the geomagnetic equator. *J. Geophys. Res.*, **117**, A08337, doi: 10.1029/2012JA017692. [Link]

Prabhakaran Nayar, S. R., T. J. Mathew, C. V. Sreehari, S. G. Sumod, C. V. Devasia, S. Ravindran, V. Sreeja, T. Kumar Pant, and R. Sridharan, 2009: Electrodynamics of the equatorial F-region ionosphere during pre-sunrise period. *Ann. Geophys.*, **27**, 107-111, doi: 10.5194/angeo-27-107-2009. [Link]

Ratcliffe, J. A., 1972: An Introduction to Ionosphere and Magnetosphere, Cambridge University Press, 266 pp.

Rishbeth, H. and C. S. G. K. Setty, 1961: The *F*-layer at sunrise. *J. Atmos. Terr. Phys.*, **20**, 263-276, doi: 10.1016/0021-9169(61)90205-7. [Link]

APPENDIX A.

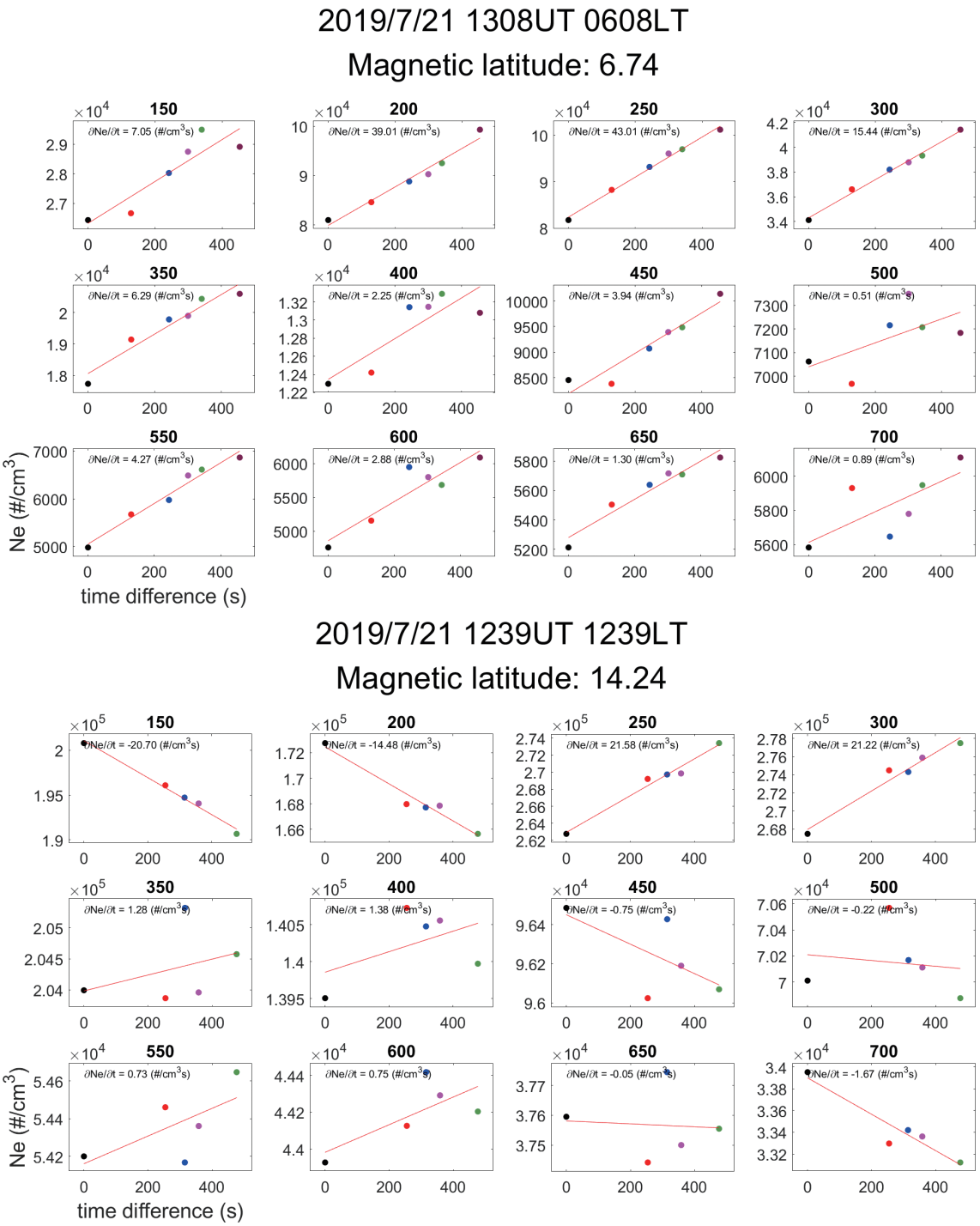

Fig. A1. Similar to the panel (d) in Figs. 3 - 7, the temporal variation of the electron density at various height during the five events. The colors denote the number of the F7/C2 satellites.

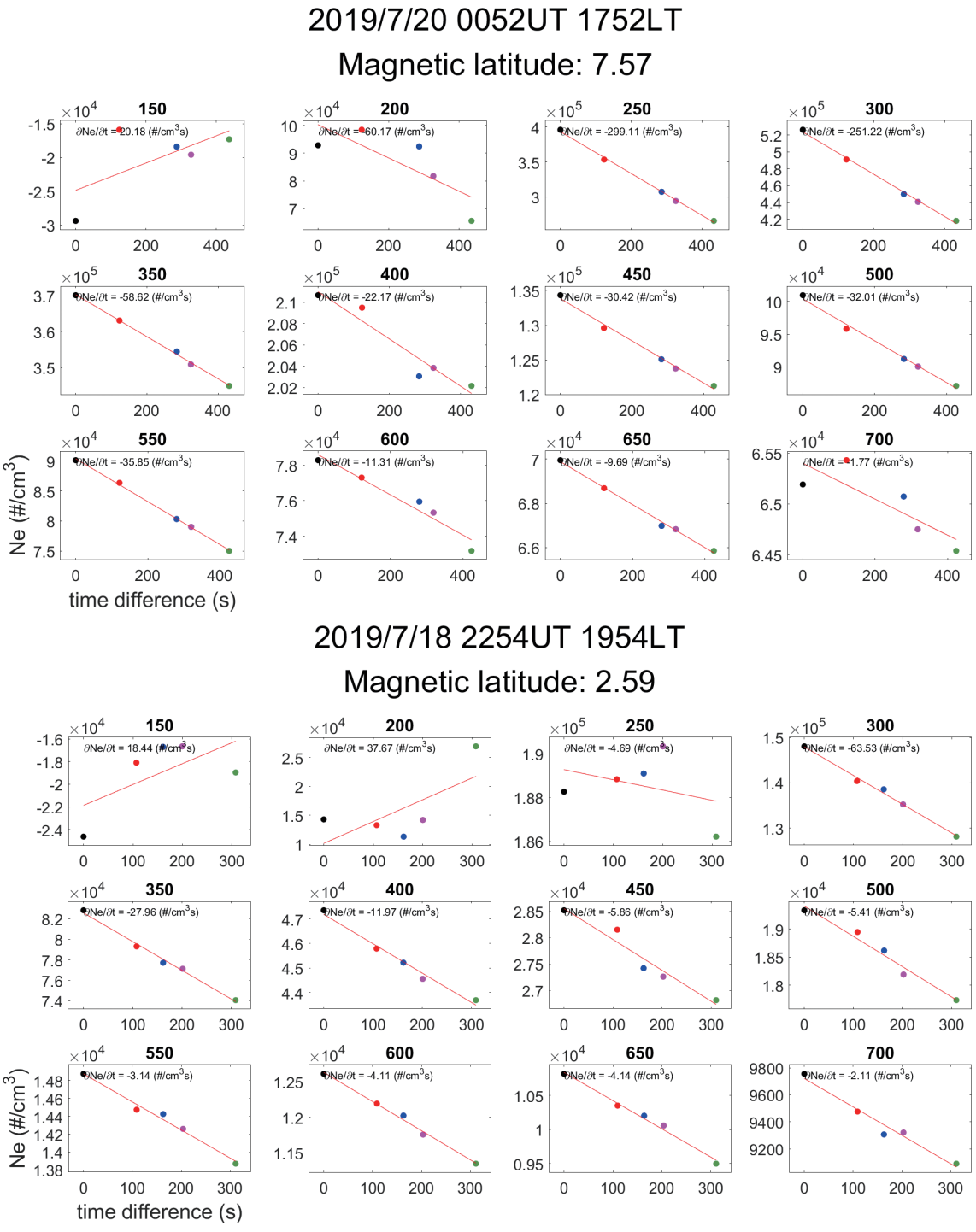

Fig. A1. (Continued)

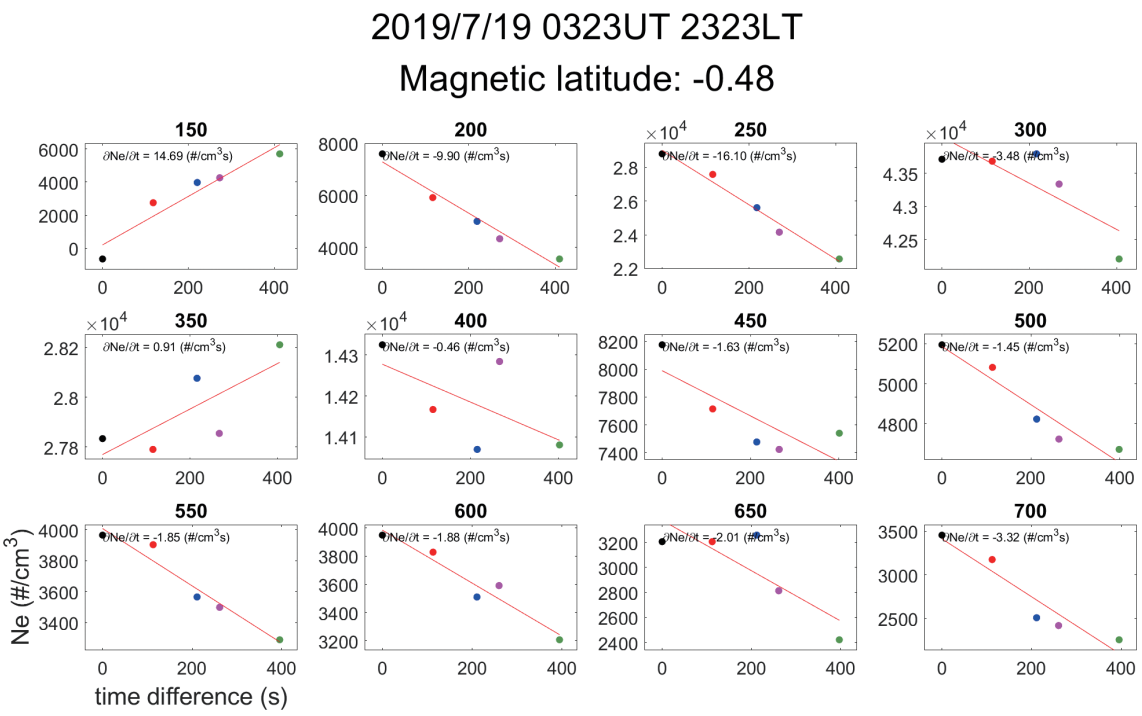

Fig. A1. (Continued)